Osteoporosis International (2018) 29:665–673
https://doi.org/10.1007/s00198-017-4328-1

Early diagnosis of osteoporosis using radiogrammetry and texture analysis from hand and wrist radiographs in Indian population

A. S. Areeckal[1] · N. Jayasheelan[2] · J. Kamath[2] · S. Zawadynski[3] · M. Kocher[4] · S. David S.[1]

Received: 6 June 2017 / Accepted: 24 November 2017 / Published online: 3 December 2017

Abstract

Summary We propose an automated low cost tool for early diagnosis of onset of osteoporosis using cortical radiogrammetry and cancellous texture analysis from hand and wrist radiographs. The trained classifier model gives a good performance accuracy in classifying between healthy and low bone mass subjects.

Introduction We propose a low cost automated diagnostic tool for early diagnosis of reduction in bone mass using cortical radiogrammetry and cancellous texture analysis of hand and wrist radiographs. Reduction in bone mass could lead to osteoporosis, a disease observed to be increasingly occurring at a younger age in recent times. Dual X-ray absorptiometry (DXA), currently used in clinical practice, is expensive and available only in urban areas in India. Therefore, there is a need to develop a low cost diagnostic tool in order to facilitate large-scale screening of people for early diagnosis of osteoporosis at primary health centers.

Methods Cortical radiogrammetry from third metacarpal bone shaft and cancellous texture analysis from distal radius are used to detect low bone mass. Cortical bone indices and cancellous features using Gray Level Run Length Matrices and Laws' masks are extracted. A neural network classifier is trained using these features to classify healthy subjects and subjects having low bone mass.

Results In our pilot study, the proposed segmentation method shows 89.9 and 93.5% accuracy in detecting third metacarpal bone shaft and distal radius ROI, respectively. The trained classifier shows training accuracy of 94.3% and test accuracy of 88.5%.

Conclusion An automated diagnostic technique for early diagnosis of onset of osteoporosis is developed using cortical radiogrammetric measurements and cancellous texture analysis of hand and wrist radiographs. The work shows that a combination of cortical and cancellous features improves the diagnostic ability and is a promising low cost tool for early diagnosis of increased risk of osteoporosis.

Keywords Distal radius · Metacarpal · Osteoporosis · Radiogrammetry · Texture analysis

Electronic supplementary material The online version of this article (https://doi.org/10.1007/s00198-017-4328-1) contains supplementary material, which is available to authorized users.

✉ A. S. Areeckal
anu_shaju_ec13f06@nitk.edu.in

[1] Department of Electronics and Communication Engineering, National Institute of Technology Karnataka, Surathkal, Karnataka, India

[2] Department of Orthopedics, Kasturba Medical College, Manipal University, Mangalore, Karnataka, India

[3] Nuclear Medicine Service, Hôpitaux Universitaires de Genève (HUG), Geneva, Switzerland

[4] Department of Industrial Technologies, Haute École d'Ingénierie et de Gestion du Canton de Vaud (HEIG-VD), Yverdon-les-Bains, Switzerland

Introduction

Osteoporosis is the second most common diseases of the world, next to cardiovascular diseases. According to the World Health Organization (WHO), osteoporosis is most accurately diagnosed by the measurement of bone mineral density (BMD) using dual X-ray absorptiometry (DXA) [1]. However, it is expensive and not widely available in low economies [2]. Therefore, in order to facilitate large-scale screening of people for early diagnosis of reduction in bone mass, it is necessary to develop a low cost diagnostic tool that could be used at primary health centers as a pre-screening tool.

Analysis of bone characteristics from radiographs can be used as a low cost alternative to DXA, due to the low acquisition cost and wide availability of X-ray machines. Radiogrammetry is a

technique by which measurements of cortical bone such as length, cortical thickness, area etc. are taken from radiographs [3–5]. The thickness of cortical bone decreases with reduction in bone mass. Thus, radiogrammetric measurement is useful in detecting loss of bone mass. However, radiogrammetry alone cannot accurately measure bone loss, as it explains the variability of the cortical bone only. Since cancellous bone structure undergoes changes much earlier than cortical bone during the onset of osteoporosis, analysis of the cancellous bone texture would give us a more sensitive measurement for early diagnosis of osteoporosis.

The objective of this paper is to explore the ability of cortical measurements and cancellous texture features to discriminate subjects with low bone mass from healthy subjects and to develop a fully automated technique to diagnose increased risk of osteoporosis using hand and wrist radiographs.

Materials and methods

Data

Data used in this work were obtained from 138 subjects in two hospitals in Karnataka, India. Fifty-eight men and 80 women in the age group 30 to 85 years were included in the study. Pregnant women and subjects undergoing glucocorticoids or other medications known to alter bone characteristics for the past 3 months were excluded from the study. The study protocol was approved by the Institutional Ethics Committee, Kasturba Medical College, Mangalore, Manipal University, Karnataka, India. Informed consent was obtained from all individual participants included in the study. The demographic and anthropometric details of the subjects were recorded. BMD of lumbar spine of all the subjects were measured using GE Lunar DXA densitometer. Postero-anterior (PA) view of hand and wrist radiographs of either left or right hand of the same subjects were obtained. Fifteen X-ray images were acquired using 400 mA Allengers HF Advantage as 16-bit DICOM images with pixel dimension of 0.097 mm (with deviation index in the range − 2.25 to 3.6). The remaining X-ray images were acquired using U-Arm DR Agfa DX-D 300 with acquisition parameters: X-ray tube voltage = 52 kV, X-ray tube current = 160 mA, exposure time = 32 ms, varying source-to-object distance of 990 to 1370 mm and deviation index in the range − 8.1 to − 1.8. These images were obtained in 16-bit DICOM format with pixel dimension of 0.139 mm.

WHO has defined the criteria for diagnosis of osteoporosis based on T-scores by taking as reference the peak BMD value of Caucasian women of age 20–29 years [6]. In this work, the subjects are categorized into two groups, namely healthy group with T-score ≥ − 1 and low bone mass group (LBM) with T-score < − 1. The data collected comprises of 67 images belonging to healthy group with 32 men and 35 women (age = 45.6 ± 10.6 years) and 71 images belonging to LBM group with 26 men and 45 women (age = 52.7 ± 10.6 years). The mean height and weight of the healthy group are 161.25 ± 8.62 cm and 66.84 ± 9.58, respectively. The mean height and weight of the LBM group are 157.41 ± 6.02 cm and 58.61 ± 9.21 kg, respectively.

Proposed methodology

In this paper, a completely automated technique for detection of low bone mass is proposed by combining radiogrammetric measurements of cortical bone along with texture features of cancellous bone using hand and wrist radiographs. Automated radiogrammetry, as compared to manual radiogrammetry, removes subjective error (i.e., intra- and inter-observer variability) and improves the precision and reliability of the measurements. Cortical bone loss is determined using fully automated radiogrammetric measurements of third metacarpal bone of hand. Changes in cancellous bone structure are analyzed by texture features extracted from distal radius of wrist. Since osteoporosis is a systemic disease, the loss of bone mass can be examined from any skeletal site. Hand and wrist radiograph is chosen in our work, as it is a convenient acquisition site for patients with high morbidity and central skeletal fractures. Cortical radiogrammetry can be done on a single metacarpal bone. Third metacarpal bone is used in our work as it can be easily identified irrespective of the hand orientation (left or right). The site chosen for cancellous texture analysis is the distal radius as it is a potential site for measurement, due to the presence of a large area of cancellous bone.

Figure 1 shows a flowchart of the main processing steps of the proposed diagnostic technique. The hand radiograph is first preprocessed to remove effects of noise and non-

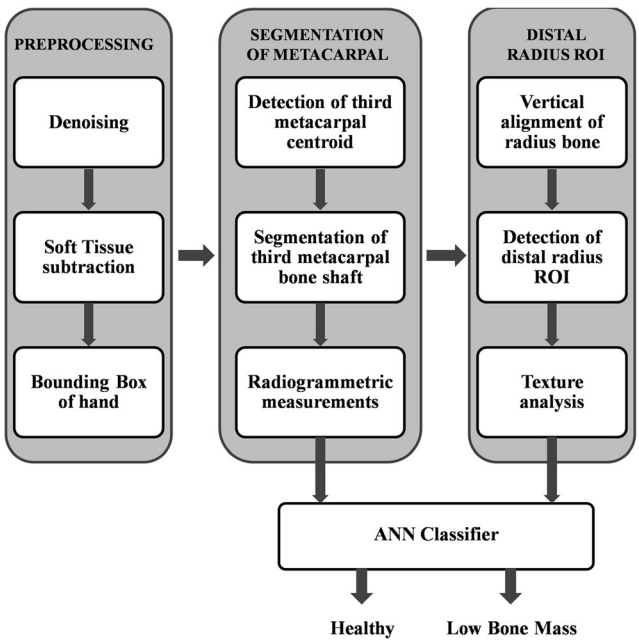

Fig. 1 Block diagram showing the proposed methodology of the automated diagnostic tool

uniform illumination. An automatic segmentation approach is used to segment the third metacarpal and distal radius region of interest (ROI), from which radiogrammetric cortical measurements and texture features are extracted respectively. These features are used to train a classifier model that can classify healthy and low bone mass groups.

Preprocessing

Prior to segmentation, the hand radiographic images have to be preprocessed, in order to remove noise and illumination variation due to different acquisition conditions. Hand X-ray images are denoised using Block Matching 3D (BM3D) method, which helps to remove noise while preventing the blurring of edges [7]. A background and soft tissue subtraction is done using a large Gaussian filter of size of 1000 pixels and standard deviation of 200, to obtain an image of the hand bone region (Fig. S1, Online Resource 1). The background subtracted image is then thresholded to get a binary image of hand bone region and the bounding box of hand is determined. The dimensions of the hand bounding box will be used for estimating the centroid of the third metacarpal bone, as described in the next section.

Automatic segmentation of third metacarpal

Third metacarpal bone is segmented from the hand bone image using mathematical morphology and watershed segmentation [8, 9]. The main steps used in the automatic segmentation of periosteal and endosteal bone edges are shown in Fig. 1. To estimate the centroid of the third metacarpal bone, two reference lines are determined from the upper border of hand bounding box and the distal radius-ulnar junction (DRUJ) line. The horizontal line containing the point of intersection of the radius and ulna bones is denoted as DRUJ line. DRUJ line is determined by finding the peaks of horizontal intensity profiles in the lower half of the hand bone binary image. The intensity profile at the intersection of radius and ulna shows a single peak in the binary image, whereas intensity profiles below DRUJ line show two distinct peaks, representing radius and ulna (Fig. S2, Online Resource 1). The image row showing a single peak in the intensity profile is taken as the DRUJ line. The mid-region of third metacarpal bone containing the centroid is then estimated by using the two reference lines. The first reference line is taken 70 mm above the DRUJ line. The second reference line is selected 125 mm below the upper boundary of the hand, determined by the hand bounding box. The distances of these reference lines were found empirically, after examining all image samples. The pixel dimension required to estimate the distances in mm is obtained from the DICOM header files in the image. The average of both the reference lines will correspond to the image row containing the centroid of third metacarpal bone. Taking into consideration the two reference lines will ensure the accurate determination of centroid for hands of all sizes. A horizontal intensity profile of this row is taken to determine the position of the centroid of third metacarpal. The profile obtained is smoothened to remove noise (Fig. S3, Online Resource 1). The smoothened profile shows five prominent intensity peaks corresponding to the five metacarpal bones. The third peak of the smoothened intensity profile is selected as the centroid of the third metacarpal bone. This centroid is used to determine markers for watershed segmentation. The periosteal and endosteal edges of the third metacarpal bone are then segmented using marker-controlled watershed method, as described in our previous work [10].

Metacarpal radiogrammetry

The bone shaft of the segmented third metacarpal bone is used for cortical radiogrammetry, as shown in Fig. 2. From the segmented periosteal and endosteal edges, average cortical width (CW) and medullary width (MW) along the metacarpal bone shaft are measured. Various bone indices such as combined cortical thickness (CCT), cortical area (CA), transverse cortical area (A), Barnett Nordin Index (BNI), and Metacarpal Index (MCI) are automatically calculated from the radiogrammetric measurements [3, 5]. CCT is measured as the average cortical thickness of the medial and lateral cortical bone of the third metacarpal measured at 100 measurement lines within the third metacarpal bone shaft. Equations used for the calculation of bone indices are given in Online Resource 3.

Automated extraction of distal radius ROI

Texture analysis of cancellous bone is carried out on a circular ROI of the distal radius. To segment the circular ROI, the

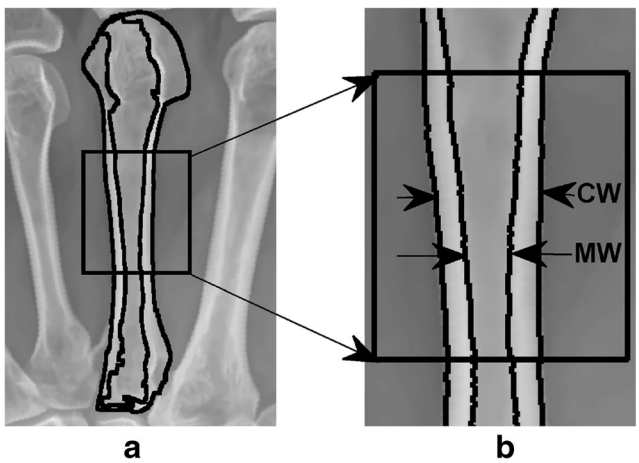

Fig. 2 Automatic segmentation of third metacarpal bone. **a** Segmented third metacarpal with detected bone shaft. **b** Radiogrammetric measurements from the bone shaft

radius bone is first vertically aligned. The orientation of radius bone is determined by finding the central axis of the radius bone using intensity profiles.

The approximate position of the center of circular distal radius ROI is taken 3 mm below the DRUJ line along the central axis of radius bone. The radius of circular ROI is found by determining the width of the radius bone along this row. In order to fit in the largest circle that can be inscribed in the distal radius, the upper boundary of distal radius is found by taking a vertical intensity profile along the central axis of radius bone (starting from the approximate center to 20 mm above the center towards the carpal region), as shown in Fig. 3a. All the distances are determined empirically. The highest peak along this vertical intensity profile corresponds to the upper border of distal radius. The center of the circular ROI is moved such that the circle lies in the most distal end of the radius bone. The circular ROI is segmented from the image, as shown in Fig. 3c. The largest square region contained in the circular ROI is extracted and used for texture analysis.

Texture analysis of cancellous ROI

The texture images of healthy and low bone mass groups are visually similar to the naked eye and it is often difficult to distinguish between the two groups. In order to capture the finer textural variations in these images, higher order statistics such as Gray Level Run Length Matrix (GLRLM) and Laws' masks are useful. GLRLM measures the run length characteristics of the texture. Since trabeculae are observed as elongated tubular structures, GLRLM is a good choice of texture method to characterize the trabeculae. Laws' filter masks help to filter out other texture characteristics like edges, wave, ripple and spot nature of the texture images. Hence, GLRLM and Laws' masks can be used as an effective texture analysis tool to characterize the trabeculae in the cancellous bone.

The square ROI segmented from the distal radius is preprocessed before analyzing the texture. The ROI images are resized to 150 × 150, in order to uniformly calculate GLRLM. Contrast of the image is enhanced by linear mapping of pixels to the full dynamic range. Soft tissue subtraction is employed using Gaussian filter of size 20 × 20 and standard deviation of 20, to extract the trabeculae for texture analysis (Fig. S4, Online Resource 1).

GLRLM represents the number of pixels within a connected set of pixels that have the same intensity along a particular direction [11]. Each element of GLRLM matrix stores the number of gray level runs with a specific intensity and length along a particular direction. Fine textures have more short runs with similar intensities while coarse textures have more long runs with different intensities. The background subtracted ROI image is quantized to 2^8 gray levels, because all the pixel intensities in 16 bits is not useful to calculate GLRLM. GLRLM is measured along four principal directions, 0°, 45°, 90°, and 135° to the horizontal and statistics are calculated along each direction separately. In this work, the features extracted from GLRLM are short run emphasis (SRE), long run emphasis (LRE), gray level non-uniformity (GLN), run length non-uniformity (RLN), low gray level run emphasis (LGRE), and high gray level run emphasis (HGRE). These six features are extracted from GLRLM of four directions separately, and thus a total of 24 features are obtained using GLRLM.

Laws' texture masks are filter masks created from the combination of five 1D kernel vectors of 5 pixels length, in order to assess texture properties [12]. The five kernel vectors used are level vector (L5), edge vector (E5), spot vector (S5), ripple vector (R5), and wave vector (W5). Level vector determines the center weighted local average. Edge vector acts as a gradient operator. Spot vector and ripple vector detect spots and ripples in the image. Wave vector identifies wave-like structures in the texture image. Laws' masks are used to filter the images to obtain texture images. By convolving a vertical 1D vector with a horizontal 1D vector, 25 filter masks of size 5 × 5 are generated, from which 25 filtered images are obtained (i.e., L5L5, L5E5, L5S5, etc.). The filtered images from symmetric Laws' masks (formed using the same vector combinations) are fused together to get a single texture image, as they impart the same information. i.e. L5E5 and E5L5 masked images are fused together. The filtered image formed by L5L5 is not considered for the analysis, as it is just the average of the

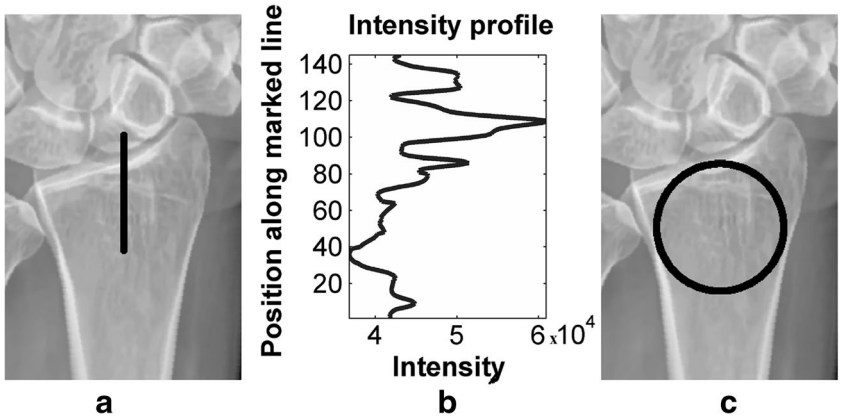

Fig. 3 Automatic estimation of upper boundary of distal radius. **a** Central axis of radius bone extending from the approximate ROI center to carpal region. **b** Intensity profile along the marked central axis to detect the upper boundary of distal radius. **c** Largest circle inscribed at the distal radius

ROI image. Therefore, a total of 14 fused texture images are obtained (i.e., L5E5, L5S5, L5R5, L5W5, E5E5, E5S5, E5R5, E5W5, S5S5, S5R5, S5W5, R5R5, R5W5, and W5W5 texture images). These fused texture images are normalized and various features such as contrast, correlation, homogeneity, and energy are calculated from all 14 texture images, resulting in a total of 56 features. The equations used for the texture feature calculations are given in Online Resource 3.

Statistical analysis

A total of 5 cortical features and 80 cancellous features are extracted using cortical radiogrammetry and texture analysis, respectively. All the 85 extracted features may not be useful for classification. So, a feature selection method using statistical tests is employed to select the most discriminating features to be used for training the classifier. Statistical significance of the extracted features of the healthy and low bone mass groups is analyzed using independent sample t test. A significance level of $p < 0.05$ is considered to be statistically significant. The cortical and cancellous features are then analyzed for correlation with DXA-BMD of lumbar spine (DXA-LS) using the Pearson correlation. The resulting highly significant and correlated features are selected as the input feature set for training the classifier.

Classifier

Classifier used in this work is a three-layer supervised artificial neural network (ANN) classifier with one hidden layer and two output nodes, corresponding to the two output classes, namely healthy and low bone mass classes. The classification results may be grouped as four outcomes: true positive (TP), false positive (FP), true negative (TN), and false negative (FN). In this work, healthy images are taken as the positive case and low bone mass samples are taken as the negative cases. TP denotes the case when a healthy subject is correctly classified as healthy. FP is the case when a subject with low bone mass is incorrectly classified as healthy. TN is the case when a diseased subject is accurately classified to the low bone mass group and FN denotes the case when healthy people are misclassified as having low bone mass. These four outcomes can be formulated into a confusion matrix, from which performance metrics such as accuracy, sensitivity, and specificity can be calculated. These performance metrics are used to evaluate the performance of the trained classifier.

For clinical use, a hand and wrist X-ray image of the patient is acquired. The proposed software automatically segments the regions of interest at the third metacarpal and distal radius, from which cortical and cancellous features are extracted. These features are then used by the trained classifier to classify the patient as either healthy or having low bone mass. The patients diagnosed with low bone mass could be referred to specialists for detailed clinical examination and treatment.

Results

This work was done using Matlab R2016b. Statistical analysis was done using the Statistical Toolbox of Matlab R2016b. ANN classifier model was trained using the Neural Network Pattern Recognition Tool of Matlab R2016b.

The third metacarpal bone and the distal radius ROI are automatically segmented from the hand and wrist radiographs and processed for feature extraction. Out of 138 images, the automatic segmentation algorithm is able to accurately detect the third metacarpal and delineate the periosteal and endosteal edges along the bone shaft in 124 images, giving an accuracy of 89.9% in accurate detection of the third metacarpal bone. The automatic radiogrammetric measurements obtained for 20 images were compared with the ground truth images obtained from orthopedicians. The comparison results show a mean absolute error of 0.11 mm (1.36%) for cortical width and 0.25 mm for medullary width (7.08%). The proposed automated approach for extraction of distal radius ROI is successful in 129 images, showing 93.5% accuracy in accurate detection of the circular ROI. After removing the poorly segmented images, the remaining 117 images are taken as the study group for feature extraction and classification. Among the 117 images, 57 belonged to healthy group (age = 45 ± 10.5 years) and 60 belonged to low bone mass group (age = 52.2 ± 9.9 years). Average heights of the healthy and LBM groups are 161.14 ± 8.43 cm and 157.07 ± 5.98 cm, respectively. Average weights of the healthy and LBM groups are 66.68 ± 9.91 kg and 58.78 ± 9.55 kg, respectively. The clinical characteristics of this study group of 117 images are given in the table (Table S1, Online Resource 2).

Five cortical radiogrammetric measurements are determined automatically from the extracted third metacarpal bone shaft. Eighty cancellous texture features are extracted from the distal radius of the wrist. To remove insignificant features and reduce the complexity of the classifier, it is necessary to reduce feature space dimension. In this work, independent sample t test is used as the feature selection method to select the most significant features to be used in the classifier. The results of the t test on the clinical parameters and the extracted features of the dataset after removal of outliers (training set) are listed in Table 1. Only those features showing a statistical significance of $p < 0.05$ are included in the table. It can be observed that all extracted cortical features are significant. CCT shows the highest discrimination between healthy and low bone mass as compared to all the features with a significance of $p < 0.0001$. Among the 80 cancellous features, 38 cancellous features are observed to be significant with t test.

Table 1 Statistical significance values of the clinical parameters and significant features using independent sample *t* test ($p < 0.05$) in the training set of the healthy and low bone mass groups

Measurements	Significant features	Healthy group (22 men and 22 women) Mean (SD)	LBM group (16 men and 27 women) Mean (SD)	Significance (*p* value)
Clinical parameters	Age (years)	44.96 (11.12)	51.49 (10.07)	0.0054[a]
	Height (cm)	161.07 (8.24)	157.51 (5.93)	0.0240
	Weight (kg)	67.47 (9.91)	60.69 (8.51)	0.0010[b]
	BMI (kg/m^2)	26.06 (3.77)	24.48 (3.27)	0.0410
	DXA-BMD (g/cm^2)	1.1879 (0.0695)	0.9536 (0.0818)	2.9385e-24[c]
	T-score	− 0.0861 (0.5680)	− 2.0512 (0.6501)	2.3792e-25[c]
Cortical measurements	CCT (mm)	4.5 (0.6)	3.8 (0.5)	2.6744e-06[c]
	CA (mm^2)	42.9 (7.0)	35.8 (6.5)	0.0001[b]
	A (mm^2)	53.4 (11.5)	48.1 (9.1)	0.0297
	BNI	54.5 (8.1)	48.9 (6.8)	0.0046[a]
	MCI	0.7587 (0.0374)	0.7705 (0.0171)	0.0315
Cancellous measures	GLRLM_0_SRE	0.2210 (0.0139)	0.2106 (0.0150)	0.0013[a]
	GLRLM_0_GLN	4964.5 (97.97)	5.0301 (108.29)	0.0042[a]
	GLRLM_0_RLN	379.78 (51.36)	347.46 (49.56)	0.0038[a]
	GLRLM_0_LGRE	0.8420 (0.0062)	0.8481 (0.0078)	0.0001[a]
	GLRLM_45_SRE	0.2454 (0.0117)	0.2374 (0.0146)	0.0059[a]
	GLRLM_45_GLN	5087.0 (106.48)	5136.4 (98.85)	0.0285
	GLRLM_45_RLN	473.41 (49.74)	445.63 (56.31)	0.0175
	GLRLM_45_LGRE	0.8400 (0.0046)	0.8438 (0.0057)	0.0011[a]
	GLRLM_90_GLN	5098.5 (101.47)	5156.6 (109.51)	0.0126
	GLRLM_90_LGRE	0.8729 (0.0059)	0.8765 (0.0075)	0.0145
	GLRLM_135_SRE	0.2504 (0.0150)	0.2390 (0.0155)	0.0008[b]
	GLRLM_135_RLN	496.11 (66.56)	452.38 (60.29)	0.0019[a]
	GLRLM_135_LGRE	0.8396 (0.0041)	0.8436 (0.0058)	0.0004[b]
	LAWS_L5E5_CONT	1906.1 (34.1)	1893 (35.8)	0.0360
	LAWS_L5E5_CORR	− 0.0032 (0.0183)	0.0037 (0.0163)	0.0350
	LAWS_L5S5_CONT	1949.8 (41.5)	1923.9 (44.1)	0.0026[a]
	LAWS_L5S5_CORR	0.0032 (0.0195)	0.0131 (0.0199)	0.0083[a]
	LAWS_L5S5_HOM	0.0697 (0.0019)	0.0710 (0.002)	0.0012[a]
	LAWS_L5R5_CORR	0.0033 (0.0187)	0.0148 (0.02)	0.0410
	LAWS_L5W5_CONT	2128.0 (135.4)	2057.8 (145.8)	0.0373
	LAWS_L5W5_CORR	0.0015 (0.0492)	0.0361 (0.0609)	0.0067[a]
	LAWS_E5E5_CONT	1887.1 (69.8)	1845.4 (70.1)	0.0072[a]
	LAWS_E5E5_CORR	0.0109 (0.0326)	0.0253 (0.0339)	0.0424
	LAWS_E5S5_CONT	1923.9 (63.0)	1879.3 (70.1)	0.0029[a]
	LAWS_E5S5_CORR	0.0049 (0.0290)	0.0231 (0.0321)	0.0079[a]
	LAWS_E5R5_CORR	−0.0034 (0.0261)	0.0135 (0.0273)	0.0259
	LAWS_E5W5_CONT	1907.3 (82.9)	1859.3 (67.7)	0.0055[a]
	LAWS_ E5W5_CORR	0.0069 (0.0338)	0.0213 (0.0286)	0.0351
	LAWS_S5S5_CONT	1964.0 (65.6)	1916.8 (78.1)	0.0032[a]
	LAWS_ S5S5_CORR	0.0001 (0.0283)	0.0194 (0.0325)	0.0036[a]
	LAWS_ S5S5_HOM	0.0710 (0.0034)	0.0724 (0.0030)	0.0199
	LAWS_S5R5_CORR	−0.0066 (0.0249)	0.0106 (0.0281)	0.0147
	LAWS_S5W5_CONT	1865.1 (69.6)	1812.3 (66.4)	0.0005[b]
	LAWS_ S5W5_CORR	0.0111 (0.0285)	0.0316 (0.0280)	0.0006[b]
	LAWS_ S5W5_HOM	0.0717 (0.0025)	0.0729 (0.0024)	0.0096[a]
	LAWS_R5W5_CORR	0.0019 (0.0260)	0.0183 (0.0298)	0.0276
	LAWS_W5W5_ CONT	1878.9 (109.7)	1818.6 (80.0)	0.0055[a]
	LAWS_W5W5_HOM	0.0718 (0.0034)	0.0736 (0.0035)	0.0301

LBM, low bone mass, GLRLM_x_y, 'y' feature of GLRLM measured along 'x' direction to the horizontal, LAWS_u_v, 'v' feature measured from Laws' texture image 'u'

[a] $p < 0.01$, [b] $p < 0.001$, [c] $p < 0.0001$

Table 2 shows the Pearson correlation of the significant cortical and cancellous features ($p < 0.01$ using *t* test) with DXA-LS tested on the whole study group. The correlation results of all the extracted features with DXA-LS are given in the table (Table S2, Online Resource 2). Cortical features of third metacarpal bone are observed to be more correlated with DXA-LS as compared to cancellous features of the distal radius. The most highly correlated feature is CCT with

Table 2 Correlation of significant features of independent sample *t* test ($p < 0.01$) with DXA-BMD of lumbar spine using the Pearson correlation analysis

Significant features ($p < 0.01$)	Correlation	Significance (p value)
CCT	0.5632	3.8314e-11[b]
CA	0.4839	3.2371e-08[b]
BNI	0.4002	7.8116e-06[b]
GLRLM_0_SRE	0.3928	1.1840e-05[b]
GLRLM_0_RLN	0.3716	3.7151e-05[b]
GLRLM_0_LGRE	− 0.3273	0.0003[a]
GLRLM_45_SRE	0.4070	5.2590e-06[b]
GLRLM_45_LGRE	− 0.4005	7.6494e-06[b]
GLRLM_135_SRE	0.3823	2.1009e-05[b]
GLRLM_135_RLN	0.3657	5.0337e-05[b]
GLRLM_135_LGRE	− 0.3078	0.0007[a]
LAWS_E5S5_CONT	0.3368	0.0002[a]
LAWS_ E5S5_CORR	− 0.3013	0.0009[a]
LAWS_S5S5_CONT	0.3561	8.1551e-05[b]
LAWS_S5S5_CORR	− 0.3413	0.0001[a]

[a] $p < 0.001$, [b] $p < 0.0001$

correlation coefficient of $r = 0.5632$ and $p < 0.0001$. Fifteen features are found to be highly significant using *t* test and correlated with DXA-LS, as seen in Table 2.

In order to study the correlation of a linear combination of these 15 features with DXA-LS, a backward linear regression is applied. The linear regression equation obtained is given in the equation below.

$$BMD = -0.017 + 0.007 \times CA + 0.009 \times BNI + 0.001 \times GLRLM\_135\_RLN - 1.091 \times LAWS\_E5S5\_CORR \quad (1)$$

The linear regression model shows a correlation coefficient of $r = 0.671$ ($p < 0.001$) with DXA-LS. The predictor variables of the linear regression model along with its significance and collinearity statistics are summarized in the table (Table S3, Online Resource 2). Pair-wise correlation test shows low correlation between the predictor variables (Table S4, Online Resource 2).

Out of the highly significant 15 features, two features namely, contrast and correlation of Laws' texture image S5S5 is found to be highly correlated with contrast and correlation of Laws' texture image E5S5, respectively. Therefore, contrast and correlation of Laws' texture image S5S5 are discarded. The remaining 13 features are used as input feature vector for training the ANN classifier. The 117 images are divided into a training set of 73 images and a validation set of 14 images. The remaining 30 images are used as unseen data for testing. The training set is normalized before feeding to the neural network.

Two ANN classifiers are trained, one with 3 cortical features alone, and the other with 13 cortical and cancellous features combined together. The ANN classifier trained with cortical features alone is modeled with three input nodes for the cortical features, one hidden layer with three nodes and an output layer with two nodes for the two output classes. The number of hidden nodes is chosen by trial and error to obtain the maximum classification accuracy. The performance measures of the trained classifiers are shown in Table 3. The trained classifier model using the cortical features alone attained a training and validation accuracy of 81.6%. This trained classifier is then tested on 30 test images, which shows an accuracy of 73.3%. The overall accuracy achieved by the trained ANN classifier with cortical features is 79.5% with a sensitivity of 78.9% and specificity of 80%. The ANN classifier trained with cortical and cancellous features together is designed with an input layer with 13 nodes, one hidden layer with eight nodes and two output nodes. This classifier shows a training accuracy of 94.3% and test accuracy of 88.5%. The overall accuracy of the trained classifier is 93.2% with sensitivity of 91.2% and specificity of 95%. As observed in Table 3, inclusion of cancellous features improves the performance of the trained classifier.

Discussion

Digital X-ray radiogrammetry (DXR) is a widely used computerized technique that takes radiogrammetric measurements

Table 3 Performance evaluation of the trained classifier model

Features	Dataset	Samples	TP	FP	TN	FN	Sensitivity (%)	Specificity (%)	Accuracy (%)
Cortical features ($n = 3$)	Training	87	34	8	37	8	81	82.2	81.6
	Testing	30	11	4	11	4	73.3	73.3	73.3
	Overall	117	45	12	48	12	78.9	80	79.5
Cortical and cancellous features ($n = 13$)	Training	87	40	2	42	3	95.2	93.3	94.3
	Testing	30	12	3	15	0	80	100	88.5
	Overall	117	52	5	57	3	91.2	95	93.2

TP true positive; *FP* false positive; *TN* true negative; *FN* false negative

of the second, third, and fourth metacarpal bones to estimate BMD. It shows a good correlation with BMD determined from DXA [4]. Our work is different from DXR in that this proposed technique explores the ability of cortical measurements from a single metacarpal bone to detect bone loss. This work uses a classification technique to detect people with low bone mass. Moreover, DXR does not take into account the texture variations in the cancellous bone. This could be a limitation in identifying patients at the onset of osteoporosis. Previous works have reported the potential role of cancellous features in improving the diagnostic accuracy of onset of osteoporosis [13, 14]. Hence, in this work, we combine the cortical features extracted from third metacarpal with cancellous features extracted from distal radius and analyze its ability to characterize bone structure and detect low bone mass.

CCT of third metacarpal bone shows a significant positive correlation with DXA-LS ($r = 0.56$, $p < 0.0001$). The positive correlation implies that the thickness of cortical bone increases with BMD and hence a thicker cortical bone indicates a stronger bone. Cortical area, CA, shows a highly significant correlation of $r = 0.48$ ($p < 0.0001$) with DXA-LS. BNI is calculated as CCT normalized by the average cortical width of the metacarpal shaft. BNI also shows a highly significant correlation of $r = 0.4$ ($p < 0.0001$).

Texture analysis methods used for the analysis of cancellous bone structure at the distal radius are GLRLM and Laws' texture masks. The significant features extracted using GLRLM are SRE, GLN, RLN and LGRE. SRE measures the distribution of short runs and is large for fine textures, while LRE measures the occurrence of long runs and is large for coarse structural textures. SRE shows a good correlation with DXA-LS ($r = 0.39$, $r = 0.4$, and $r = 0.38$ along 0°, 45°, and 135° to the horizontal). GLN measures the similarity of gray level values throughout the image. GLN is lower if the gray level values are similar throughout the image. GLN is found to be significant between the two groups using t test with $p < 0.05$. RLN measures the non-uniformity of the length of runs in the image. RLN is lower if run lengths are similar throughout the image. RLN is significantly correlated with DXA-LS along 0° and 135° to the horizontal ($r = 0.37$). LGRE and HGRE are used to distinguish texture images that have the same values for SRE and LRE but have differences in the distribution of gray levels in the image. LGRE shows a negative correlation of $r = -0.33$, $r = -0.4$ and $r = -0.31$ along 0°, 45° and 135° to the horizontal, respectively.

The features extracted from Laws' masks are contrast, correlation, homogeneity and energy. Contrast measures the intensity contrast between a pixel and its neighbor over the whole image. It increases as the density of the trabeculae increases. Thus contrast is higher for healthy group as compared with low bone mass group. Contrast of texture images of E5S5 and S5S5 masks are found to be correlated with DXA-LS ($r = 0.34$ and $r = 0.36$, respectively). Correlation measures how correlated a pixel is to its neighbor over the entire image. It is also a measure of image linearity and will be high if an image contains a high amount of linear structure. Correlation values of texture images of E5S5 and S5S5 masks is negatively correlated with DXA-LS ($r = -0.3$ and $r = -0.34$ respectively). Homogeneity measures the closeness of the pixel value distribution in the image to the diagonal of the image matrix. It measures the similarity of the spatially close image structures. A higher homogeneity value indicates a homogenous image. Energy is defined as the sum of square of the image pixel values. It measures the regularity of patterns of the pixels. Energy is higher for a homogenous image and smaller for images with frequent and repeated patterns.

Multivariate analysis using backward linear regression of the significant cortical and cancellous features shows a good correlation with DXA-LS ($r = 0.671$, $p < 0.001$). The correlation of DXR-BMD with DXA-LS is reported to be $r = 0.62$ [4]. This shows that a combination of cortical and cancellous features will help in increasing the ability to detect low bone mass.

The performance of the trained classifier is evaluated by its accuracy, sensitivity and specificity. Sensitivity and specificity indicates the ability of the classifier to correctly identify true positive cases and true negative cases, respectively. The trained ANN classifier using both cortical and cancellous features shows a test accuracy of 88.5% with sensitivity of 80% and specificity of 100%. The inclusion of cancellous features along with the cortical features increases the test accuracy from 73.3 to 88.5%.

The proposed automated diagnostic tool has certain limitations. The proposed segmentation method failed for 21 images. The failed images include X-ray images acquired with high or low exposure, resulting in bone edges that are not very distinct. Some images failed due to improper binarization of hand bone region, resulting in wrong detection of the DRUJ line. The accuracy of the segmentation method could be improved by using contrast enhancement techniques. This work is a pilot study. The initial results of classification with the sample study group are promising and needs to be validated on a larger population. In this work, two statistical texture methods, GLRLM and Laws' masks are used for texture analysis. As part of our ongoing research study, analysis of cancellous bone using other texture analysis techniques and its ability to further improve the diagnostic accuracy is being explored. In the next phase of our study, we also plan to develop an ANN classifier that can classify subjects as healthy, osteopenic or osteoporotic, as is done in clinical practice using DXA.

In conclusion, an automated diagnostic technique for detection of subjects with low bone mass using cortical radiogrammetric measurements and cancellous texture features from hand and wrist radiographs has been proposed. The proposed segmentation method showed 89.9% accuracy in detecting the third metacarpal bone shaft and 93.5% accuracy in extraction of distal radius ROI. Comparison of the automated radiogrammetric measurements with ground truth shows a mean

absolute error of 0.11 mm (1.36%) for cortical width and 0.25 mm for medullary width (7.08%). Cortical bone indices such as CCT, CA, etc. and cancellous texture features from GLRLM and Laws' masks were extracted. The ability of the extracted cortical and cancellous features to discriminate healthy and low bone mass groups was shown using ANN classifier. Out of 85 features extracted, 15 features were significant with $p < 0.01$ using independent sample t test and correlated to DXA-BMD with $p < 0.001$. CCT was found to be the most significantly correlated feature with DXA-LS. Thirteen highly significant and correlated features were selected to train the ANN classifier, which showed a training accuracy of 94.3% and test accuracy of 88.5%. Even though the image processing techniques used in this work were implemented in Matlab, the codes used for the processing can be converted to executable codes that could be integrated to the X-ray imaging system. Hence, this work demonstrates that a combination of cortical and cancellous features from radiographs can be promising as a cost-effective tool for large scale screening of population for early diagnosis of osteoporosis at primary health centers in non-urban areas in developing countries like India. After the initial screening, the high-risk group can be referred to specialists for detailed clinical examination and treatment.

Acknowledgements We thank the Department of Orthopedics, District Wenlock Hospital, Mangalore, Karnataka, India, and Tejaswini Hospital, Mangalore, Karnataka, India, for their great help and support in acquiring the data used for this work. We thank Technical Education Quality Improvement Program (TEQIP), National Institute of Technology Karnataka, Surathkal, Karnataka, India, for providing the required fund for the data collection. We also thank Dr. Sumathi K., Associate Professor, Department of Mathematics, Manipal Institute of Technology, Manipal University, Karnataka, India, for her help in the data analysis. We would like to thank the reviewers for their valuable suggestions and comments which has improved the quality of the paper.

Compliance with ethical standards

Ethical approval All procedures performed in studies involving human participants were in accordance with the ethical standards of Institutional Ethics Committee, Kasturba Medical College, Mangalore, Manipal University, Karnataka, India, and with the 1964 Helsinki declaration and its later amendments or comparable ethical standards.

Conflicts of interest None.

References

1. Kanis JA (2008) Assessment of osteoporosis at the primary health care level. Technical Report. WHO Collaborating Centre for Metabolic Bone Diseases, University of Sheffield, Sheffield, UK
2. Asia-Pacific Regional Audit (2013) Epidemiology, costs and burden of osteoporosis in 2013. International Osteoporosis Foundation. https://www.iofbonehealth.org/data-publications/regional-audits/asia-pacific-regional-audit. Accessed 1 Jun 2017
3. Barnett E, Nordin BEC (1960) The radiological diagnosis of osteoporosis: a new approach. Clin Radiol 11(3):166–174. https://doi.org/10.1016/S0009-9260(60)80012-8
4. Rosholm A, Hyldstrup L, Baeksgaard L, Grunkin M, Thodberg HH (2001) Estimation of bone mineral density by digital X-ray radiogrammetry: theoretical background and clinical testing. Osteoporos Int 12(11):961–969. https://doi.org/10.1007/s001980170026
5. Thodberg HH, Van Rijn RR, Tanaka T, Martin DD, Kreiborg S (2010) A paediatric bone index derived by automated radiogrammetry. Osteoporos Int 21(8):1391–1400. https://doi.org/10.1007/s00198-009-1085-9
6. Kanis JA, Adachi JD, Cooper C, Clark P, Cummings SR, Diaz-Curiel M, Harvey N, Hiligsmann M, Papaioannou A, Pierroz DD, Silverman SL (2013) Standardising the descriptive epidemiology of osteoporosis: recommendations from the epidemiology and quality of life working group of IOF. Osteoporos Int 24(11):2763–2764. https://doi.org/10.1007/s00198-013-2413-7
7. Dabov K, Foi A, Katkovnik V, Egiazarian K (2007) Image denoising by sparse 3-D transform-domain collaborative filtering. IEEE Trans Image Process 16(8):2080–2095. https://doi.org/10.1109/TIP.2007.901238
8. Soille P (2004) Morphological image analysis: principles and applications. Springer-Verlag, Berlin Heidelberg. https://doi.org/10.1007/978-3-662-05088-0
9. Meyer F (1994) Topographic distance and watershed lines. Signal Process 38(1):113–125. https://doi.org/10.1016/0165-1684(94)90060-4
10. Areeckal AS, David SS, Kocher M, Jayasheelan N, Kamath J (2016) Fully automated radiogrammetric measurement of third metacarpal bone from hand radiograph. In Signal Processing and Communications (SPCOM), 2016 International Conference on IEEE 1-5. https://doi.org/10.1109/SPCOM.2016.7746608
11. Tang X (1998) Texture information in run-length matrices. IEEE Trans Image Process 7(11):1602–1609. https://doi.org/10.1109/83.725367
12. Laws KI (1980) Textured image segmentation. PhD Dissertation, University of Southern California Los Angeles Image Processing Institute
13. Lee S, Lee JW, Jeong JW, Yoo DS, Kim S (2008) A preliminary study on discrimination of osteoporotic fractured group from nonfractured group using support vector machine. In Engineering in Medicine and Biology Society (EMBS), 30th Annual International Conference of the IEEE 474–477. https://doi.org/10.1109/IEMBS.2008.4649193
14. Vokes T, Lauderdale D, Ma SL, Chinander M, Childs K, Giger M (2010) Radiographic texture analysis of densitometric calcaneal images: relationship to clinical characteristics and to bone fragility. J Bone Miner Res 25(1):56–63. https://doi.org/10.1359/jbmr.090714